
This is an electronic reprint of the original article.
This reprint may differ from the original in pagination and typographic detail.

Shah, M. A.K.Yousaf; Rauf, Sajid; Mushtaq, Naveed; Zhu, Bin; Tayyab, Zuhra; Yousaf, Muhammad; Hanif, Muhammad Bilal; Lund, Peter D.; Lu, Yuzheng; Asghar, Muhammad Imran

**Novel Perovskite Semiconductor Based on Co/Fe-Codoped LBZY
($\text{La}_{0.5}\text{Ba}_{0.5}\text{Co}_{0.2}\text{Fe}_{0.2}\text{Zr}_{0.3}\text{Y}_{0.3}\text{O}_{3-\delta}$) as an Electrolyte in Ceramic Fuel Cells**

Published in:
ACS Applied Energy Materials

DOI:
[10.1021/acsaem.1c00599](https://doi.org/10.1021/acsaem.1c00599)

Published: 28/06/2021

Document Version
Publisher's PDF, also known as Version of record

Published under the following license:
CC BY

Please cite the original version:

Shah, M. A. K. Y., Rauf, S., Mushtaq, N., Zhu, B., Tayyab, Z., Yousaf, M., Hanif, M. B., Lund, P. D., Lu, Y., & Asghar, M. I. (2021). Novel Perovskite Semiconductor Based on Co/Fe-Codoped LBZY ($\text{La}_{0.5}\text{Ba}_{0.5}\text{Co}_{0.2}\text{Fe}_{0.2}\text{Zr}_{0.3}\text{Y}_{0.3}\text{O}_{3-\delta}$) as an Electrolyte in Ceramic Fuel Cells. *ACS Applied Energy Materials*, 4(6), 5796-5806. <https://doi.org/10.1021/acsaem.1c00599>

This material is protected by copyright and other intellectual property rights, and duplication or sale of all or part of any of the repository collections is not permitted, except that material may be duplicated by you for your research use or educational purposes in electronic or print form. You must obtain permission for any other use. Electronic or print copies may not be offered, whether for sale or otherwise to anyone who is not an authorised user.

Novel Perovskite Semiconductor Based on Co/Fe-Codoped LBZY ($\text{La}_{0.5}\text{Ba}_{0.5}\text{Co}_{0.2}\text{Fe}_{0.2}\text{Zr}_{0.3}\text{Y}_{0.3}\text{O}_{3-\delta}$) as an Electrolyte in Ceramic Fuel Cells

M. A. K. Yousaf Shah,[▽] Sajid Rauf,[▽] Naveed Mushtaq,[▽] Bin Zhu,* Zuhra Tayyab, Muhammad Yousaf, Muhammad Bilal Hanif, Peter D. Lund, Yuzheng Lu,* and Muhammad Imran Asghar*

Cite This: *ACS Appl. Energy Mater.* 2021, 4, 5798–5808

Read Online

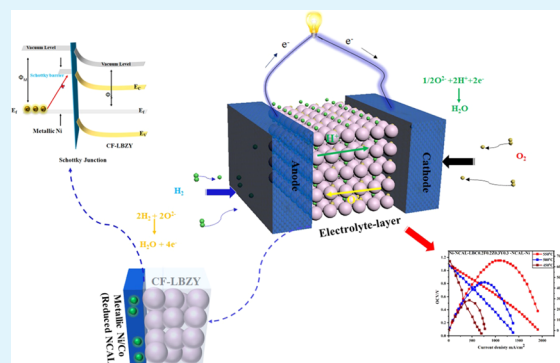
ACCESS |

Metrics & More

Article Recommendations

ABSTRACT: Introducing triple-charge ($\text{H}^+/\text{O}^{2-}/\text{e}^-$) conducting materials is a promising alternative to modify a cathode as an electrolyte in advanced ceramic fuel cells (CFC). Herein, we designed a novel triple-charge conducting perovskite-structured semiconductor $\text{Co}_{0.2}/\text{Fe}_{0.2}$ -codoped $\text{La}_{0.5}\text{Ba}_{0.5}\text{Zr}_{0.3}\text{Y}_{0.3}\text{O}_{3-\delta}$ (CF-LBZY) and used as an electrolyte and an electrode. CF-LBZY perovskite as an electrolyte exhibited high ionic (O^{2-}/H^+) conductivity of 0.23 S/cm and achieved a remarkable power density of 656 mW/cm² at 550 °C. X-ray photoelectron spectroscopy (XPS) analysis revealed that the Co/Fe codoping supports the formation of oxygen vacancies at the B-site of a perovskite structure. Besides, using CF-LBZY as a cathode, the fuel cell delivered 150 and 177 mW/cm² at 550 °C, respectively, where Y-doped BaZrO₃ and Sm-doped ceria (SDC) were used as electrolytes. During the fuel-cell operation, H^+ injection into the CF-LBZY electrolyte may suppress electronic conduction. Furthermore, the metal–semiconductor junction (Schottky junction) has been proposed by considering the work function and electron affinity to interpret short-circuiting avoidance in our device. The current systematic study indicates that triple-charge conduction in CF-LBZYO_{3-δ} has potential to boost the electrochemical performance in advanced low-temperature fuel-cell technology.

KEYWORDS: triple-charge conduction, Co/Fe- $\text{La}_{0.5}\text{Ba}_{0.5}\text{Zr}_{0.3}\text{Y}_{0.3}\text{O}_{3-\delta}$ (CF-LBZY), ceramic fuel cells, electrolyte, electrode, semiconductor, Schottky junction



1. INTRODUCTION

Low-temperature ceramic fuel cells (LT-CFCs) are known as a potential emerging clean energy technology. The CFCs rely on either proton and oxygen ion conductors or a hybrid conductor as an electrolyte material to enable low-temperature operation. Lowering the operating temperature is one of the main requirements for the current (SOFC/CFC) fuel cell research and development (R&D).^{1–3} Both Ohmic (electrolyte) and kinetic (electrode polarization) losses significantly increase with decreasing temperatures, which must be addressed to enable operation at a lower temperature (<600 °C). The Ohmic loss can be decreased by reducing the electrolyte thickness⁴ and developing electrolyte materials with high ionic conductivity at low temperatures.^{5–8}

The recent progress in perovskite-structured oxide proton conductors such as yttrium-doped BaZrO₃ (BZY) showed that the incorporation of protons suppressed the electronic conduction.⁹ Through acceptor doping in BZO, oxygen vacancies ($\text{V}_\text{o}^{\bullet\bullet}$) can be created by the substitution of multivalent cations such as (Y^{3+}) to replace Zr^{4+} .^{9,99} These

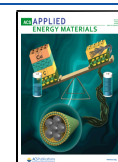
oxygen vacancies can play a critical role in the injection and transportation of protons (H^+). One mechanism for proton conduction in perovskite oxides, e.g., BZY, is by dissociative adsorption of water leading to the creation of protonic defects, indicating ionic conduction of these materials, which is closely related to oxygen vacancies. A customary way to enhance the ionic conduction (H^+/O^{2-}) is to increase the oxygen vacancies.⁹

Proton conductors are the primary materials for CFCs operating below 600 °C. La-doped PO₄, NbO₄, and CeO₂ have reasonable proton conduction at intermediate temperatures.^{10–12} The BCFZY ($\text{BaCo}_{0.4}\text{Fe}_{0.4}\text{Zr}_{0.1}\text{Y}_{0.1}\text{O}_{3-\delta}$) triple conducting cathode has also reported that doping of Co and

Received: March 2, 2021

Accepted: May 5, 2021

Published: May 19, 2021



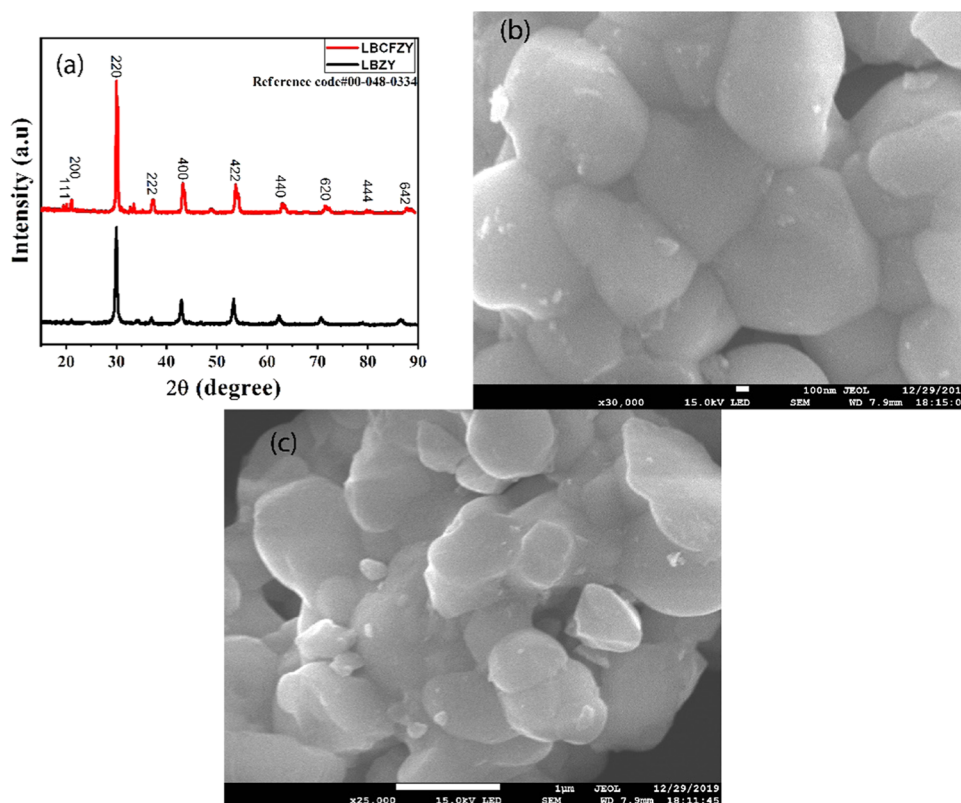


Figure 1. (a) Crystal structure analysis of CF-LBZY (XRD) data and the (b, c) scanning electron microscopy (SEM) images of CF-LBZY with different magnification scales.

Fe on the B-site of perovskite BZY (H^+/O^{2-}) exhibited a high performance of $445 \text{ mW}/\text{cm}^2$ and high conduction ($\text{H}^+/\text{O}^{2-}/\text{e}^-$) at $550 \text{ }^\circ\text{C}$.¹³ It has also been reported that via high doping of Co/Fe at the B-site, BZY still maintained its ionic conductivity and catalytic performance.¹⁴ Traditional proton-conducting CFCs use proton-conducting oxide electrolytes such as BZY and Y-doped BaCeO_3 (BCY), which have enabled operating fuel cells at low temperature.^{13,15} However, new developments on using semiconductors, e.g., SNO (SmNiO_3), STO (SrTiO_3), LST (La-SrTiO_3), TiO_2 , and ZnO , to replace commonly used BZY or BCY, show advantages in enhancing both the ionic conductivity and device performance.^{16–18} Moreover, much progress has been made in oxide materials, especially to maintain the protons, dual ions (H^+/O^{2-}), and triple-charge conduction, respectively. For example, $\text{BaZr}_{0.1}\text{Ce}_{0.7}\text{Y}_{0.1}\text{Yb}_{0.1}\text{O}_{3-\delta}$ and $\text{BaZr}_{0.1}\text{Ce}_{0.7}\text{Y}_{0.1}\text{Yb}_{0.1}\text{O}_{3-\delta}$ (BZCYYb) were used to function as an electrolyte with a dual-ion SOFC device and obtained peak power density (PPD) of 452 and $577 \text{ mW}/\text{cm}^2$ at operating temperatures of 700 and $500 \text{ }^\circ\text{C}$, respectively. From the above-reported literature, it can be predicted that heavily doped BZY with transition metals has still maintained the ionic conduction. These triple-charge conduction enabled the fuel cell to operate even at a low operating temperature of $350 \text{ }^\circ\text{C}$. The latest development includes semiconductor p–n heterojunction materials as available electrolytes, e.g., p- $\text{BaCo}_{0.4}\text{Fe}_{0.4}\text{Zr}_{0.1}\text{Y}_{0.1}\text{O}_{3-\delta}$ (BCFZY) and n- ZnO as electrolytes.¹⁹ The formation of a heterostructure and band bending creates a built-in electric field that helps ions to move quickly, inhibiting the electronic conduction through an electrolyte.¹⁹ These semiconductors have potential to be used as electrolytes with low activation energies $<0.6 \text{ eV}$ and high ionic (H^+/O^{2-})

conductivity $>0.1 \text{ S}/\text{cm}$ at temperatures $<600 \text{ }^\circ\text{C}$. Compared to conventional H^+ - or O^{2-} -conducting ceramic electrolytes, superionic conductivity could be achieved in the semiconductor-based ceramic electrolytes.^{19–21} So, the semiconductor electrolytes are more proficient compared to a conventional SOFC electrolyte for low temperatures.^{16,21–30} The semiconducting nature of these perovskite materials makes them attractive for LT-CFC technology. Though LT-CFCs with semiconductor materials have successfully been demonstrated,³¹ the functioning of the semiconductor-based electrolyte and the ionic transport properties, mainly the coexistence of hybrid (H^+/O^{2-}) or triple ($\text{H}^+/\text{O}^{2-}/\text{e}^-$)-conduction mechanisms, have realized superior ionic conductivity and high electrochemical performance at low operating temperature. The functional semiconductor electrolyte membranes have been characterized in LT-PCFCs and LT-SOFCs with a variety of conduction properties, such as the hybrid conduction and triple-charge conduction mechanism but not interpreted precisely, which required much attention.

In this work, we successfully demonstrated that using CF-LBZY as an electrolyte with high ionic conductivity of $0.23 \text{ S}/\text{cm}^2$, the fuel cell delivered a high power density of $656 \text{ mW}/\text{cm}^2$. Simultaneously, using CF-LBZY as an electrode, where BZY and SDC were used as electrolyte membranes resulted in a power density of 177 and $150 \text{ mW}/\text{cm}^2$ at $550 \text{ }^\circ\text{C}$. The electrolyte and electrode functions of the CF-LBZY perovskite materials have been investigated based on this newly developed triple-charge functional material. Also, a metal–semiconductor-based junction known as the Schottky junction was conducted to explain the mechanism to avoid short-circuiting issues. All of the functionalities and the applied strategy make it promising for advanced CFC science and technology.

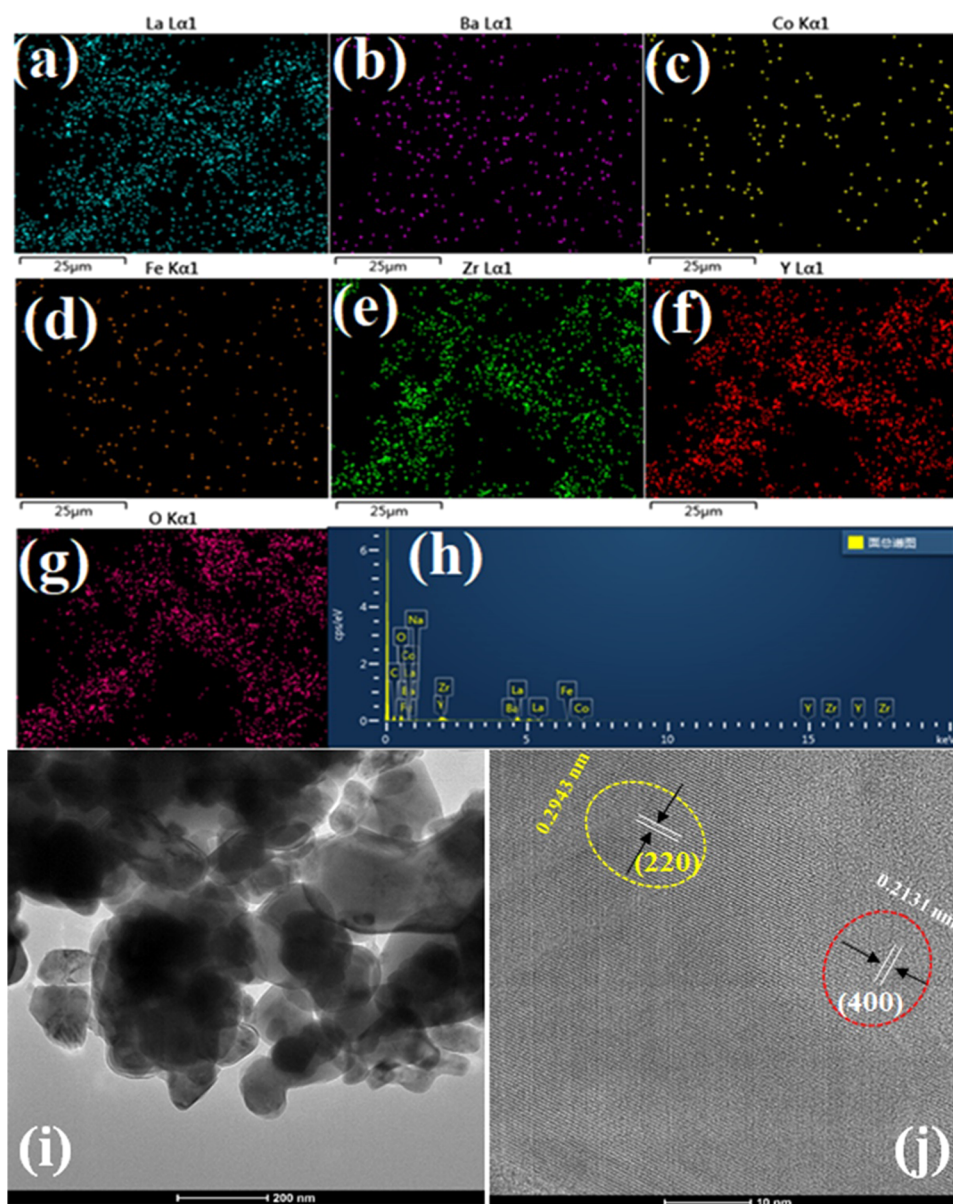


Figure 2. EDS elemental mapping region of the CF-LBZY membrane of the electrolyte cell at 550 °C: (a) La, (b) Ba, (c) Co, (d) Fe, (e) Zr, (f) Y, and (g) O and (h) elemental compositions. (i, j) TEM images and lattice fringes of CF-LBZY.

2. EXPERIMENTAL SECTION

2.1. Synthesis of Material. In a typical procedure, CF-LBZY was synthesized by coprecipitation hydrothermal techniques using a stoichiometry amount of $\text{La}(\text{NO}_3)_3$ (Sigma 99.9%), $\text{Ba}(\text{NO}_3)_2$ (Sigma 99.9%), $\text{Co}(\text{NO}_3)_2$ (Sigma 99.9%), $\text{Fe}(\text{NO}_3)_3$ (Sigma 99.9%), and nitrates of yttrium and zirconium. All nitrates were dissolved in a beaker containing 500 mL of water sequentially under a stirrer. Then, an appropriate amount of a precipitating agent, Na_2CO_3 solution, was added dropwise into the solution yielding the precipitate. The precipitate was then filtered subsequently, placed in a thermal bottle at 250 °C for 2 h, and then placed in an oven at 120 °C overnight. The dried precursor was then calcined at 1150 °C for 7 h. Finally, we obtained the desired solution, CF-LBZY oxides in a powder form, which was subjected to characterization studies. Furthermore, LBZY was synthesized following the abovementioned procedure. In addition, BCZY, BZY, and SDC were synthesized, sintered at 1000 °C, and then ground for uniform mixing. Later, it was used as a blocking layer (O^{2-}/e^-), and a protonic and oxide-ion conductive layer, respectively, in the construction of a fuel cell as mentioned in the section below.

The Ni-NCAL electrodes (anode and cathode) were prepared by mixing terpinol with NCAL powder to obtain a slurry. The slurry was then applied on the Ni foam to obtain Ni-NCAL electrodes, as reported in previous reports.^{20,32} Afterward, the prepared CF-LBZY semiconductor oxide was applied as an electrolyte and sandwiched between two Ni foams covered by NCAL used as an electrode. After that, the cell containing two processes hydrogen oxidation reaction (HOR), oxygen reduction reaction (ORR) of electrodes, electrolyte, pressed uniaxially under 200 MPa pressure to obtain the pellet of 1.5 mm thickness, an active surface area roughly around 0.64 cm² and 13 mm diameter. The electrolyte was approximately of 500 μm in thickness. All fuel cells, including Ni-NCAL/CF-LBZY/NCAL-Ni, Ni-NCAL/LBZY/NCAL-Ni, Ni-NCAL/BCZY/CF-LBZY/BCZY/NCAL-Ni, and Ni-CF-LBZY/SDC/BZY/NCAL-Ni, were sintered before the measurements at 600° to prevent them from cracking and other side effects during the fuel-cell performance; consequently, the sliver paste was applied on both sides of the cell to collect the current.

2.2. Characterization Techniques. The crystalline phase and the structure of the current sample were recorded via an X-ray diffractometer with $\text{Cu K}\alpha$ radiation ($\lambda = 1.54060 \text{ \AA}$, voltage ~ 45 kV,

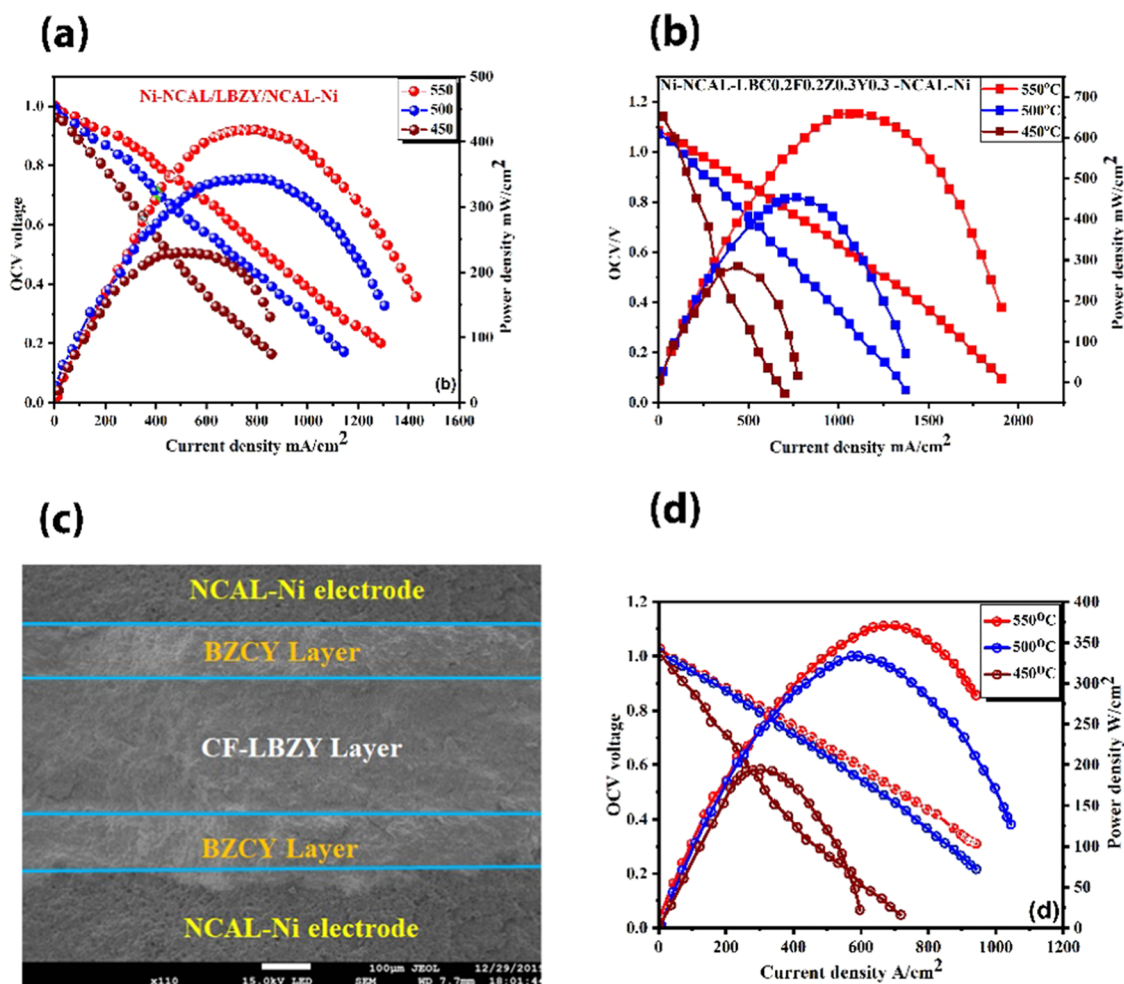


Figure 3. (a) Fuel-cell performance of LBZY cell materials, (b) fuel-cell performance of CF-LBZY cell materials, and the (c) cross-sectional SEM view of the O^{2-}/e^- blocking cell in the configuration of NCAL-Ni/BCZY/CF-LBZY/BCZY/NCAL-Ni. (d) I - V characteristics of Ni-NCAL/BCZY/CF-LBZY/BCZY/NCAL-Ni cell materials at 450, 500, and 550 °C with H_2 at the anode and flowing air at the cathode.

and current ~ 40 mA). Scanning electron microscopy (SEM) was performed to characterize the particles' size and morphology. Also, transmission electron microscopy (TEM, JEOL, JEM, 2100F) was performed to study in detail the morphology of microstructure materials, which usually operates under an accelerating voltage of 200 kV.

Electrochemical impedance spectroscopy (EIS) of the given cell was performed using an electrochemical workstation (Gamry Reference 3000, Gamry Instruments, Warminster, PA) under different gas environments like fuel gas and air. These experiments were performed at an open-circuit voltage (OCV) and a frequency range of 0.1 – 10^5 Hz. Before the EIS measurements, fuel-cell performance was measured on the following device (IT8511, ITECH Electrical Co., Ltd., Nanjing, China) under ambient hydrogen gas and air at different temperature ranges (550–450 °C). Furthermore, to investigate the oxidation states, to determine the band gap of semiconductor materials, and to attain the work function of materials, X-ray photoelectron spectroscopy (XPS), UV–visible spectroscopy, and ultra-photoelectron spectroscopy (UPS) measurements were performed, respectively.

3. RESULTS AND DISCUSSION

3.1. X-ray Diffraction. Figure 1a depicts the crystalline pattern of the as-synthesized material CF-LBZY measured via X-ray diffraction. The diffraction pattern of CF-LBZY and LBZY is accurately related to the cubic perovskite structure without observing any other peaks, signifying the pure-phase

presence. The different diffraction peaks (111), (200), (220), (222), (400), (422), (440), (620), (444), and (642) are identified as a cubic perovskite structure in a space group $Pm\bar{3}m$, which is used to observe the coherence of the pattern. The Co/Fe codoping in LBZY causes a slight shift in peaks as a piece of evidence for Co–Fe doped into the structure to form a solid solution maintained in the perovskite structure. The crystalline size was calculated using the Scherrer relation $D = K\lambda/L(\cos \theta)$ relation and found to be around 48 nm.

The surface morphology was studied using a scanning electron microscope (SEM). Figure 1b,c displays the particle size of given materials varying from 100 nm to 1 μm . The energy-dispersive spectroscopy (EDS) (element mapping) of the overall view demonstrates that all elements, including La, Ba, Co, Fe, Zr, Y, and oxygen, are uniformly distributed in the CF-LBZY sample, as shown in Figure 2a–g. Also, Figure 2h shows the elemental compositions of the CF-LBZY sample. The EDS confirms that all elements are distributed uniformly in the CF-LBZY sample. Also, Figure 2i presents transmission electron microscopy (TEM) images with uniform distribution of particles at the nanoscale. The image depicts that particles at the nanoscale are well connected, which might benefit ionic transport and device performance. Furthermore, Figure 2j depicts that lattice fringes with lattice spacings of 0.2943 and

0.2131 nm correspond to the LBCFZY crystal planes (220) and (400), respectively.

3.2. Fuel-Cell Performance. To start with, the electrochemical performance of LBZY and CF-LBZY electrolytes was determined. Figure 3a,b presents the typical fuel-cell device performance of LBZY and CF-LBZY electrolytes with an NCAL/Ni symmetrical device, respectively. In the current case, LBZY and CF-LBZY are semiconducting types of electrolytes for the fuel-cell device. First, we noticed that using the semiconducting LBZY and CF-LBZY as electrolytes, the fuel cells can still gain high OCV in the range of 1.09–1.1 V for CF-LBZY and 1.02–1 V for LBZY in the temperature range from 550 to 450 °C, respectively. The power outputs are obtained in the range from 285 to 658 mW/cm² for the CF-LBZY material-based cell, while for LBZY, the output power varies from 200 to 420 mW/cm², which is lower than that of the CF-LBZY material. Such high-performance P_{\max} is mainly due to high σ_i (ionic conductivity) of the semiconducting electrolyte membrane, reduced polarization resistance, band-gap engineering, and dopants, as reported in previous reports;³² we will further discuss on this later. The OCV, current, and power output are also dependent on temperature because ionic transport and fuel-cell reactions are thermally activated processes.

The protonic performance is determined using a blocking layer (O^{2-}/e^-) BCZY, which is applied to both sides of the CF-LBZY electrolyte in the NCAL/BCZY/CF-LBZY/BCZY/NCAL configuration. Figure 3c shows the cross-sectional SEM view of the O^{2-}/e^- blocking cell with the proton BCZY filters. The BCZY filter layer (blocking layer), the CF-LBZY electrolyte, and NCAL electrodes are visibly seen in the SEM cross-sectional image.

This device delivered the performance of about 370, 333, and 194 mW/cm² with the OCV values of 1.02, 1.01, and 1 V, respectively, in the given temperature range of 550–450 °C, as depicted in Figure 3d. Subsequently, the obtained power for this cell, we can see proton contribution makes significant contributions to the fuel-cell performances, e.g., 370 vs total 658 mW/cm² at 550 °C. These results signify that the proton conduction has marked extensive contribution as oxygen ions. It has been noticed that the performance of the current material is better than other reported materials used as electrolytes.^{33,34} The reported voltage around 1.0 V demonstrates that the present electrolyte is highly dense, causing neither gas leakage nor short-circuiting problems, leading to a high power density.³⁵ The cathode side is also a more active site for the transportation of oxygen and oxygen ions through the semiconductor–electrolyte material to complete ORR to perform advanced LT-SOFC better.

3.3. Oxygen Reduction Reaction Catalytic Activity. In addition, to verify the oxygen reduction reaction (ORR) activity and triple-charge conduction pertinency as a cathode, we applied CF-LBZY to function as a cathode. In this scenario, two cells were fabricated following NCAL/SDC/CF-LBZY and NCAL/BZY/CF-LBZY structures. The CF-LBZY acts as a cathode, while SDC and BZY are oxide-ion and proton conductor electrolytes, respectively. Figure 4 shows the I – V and I – P curves of the fuel cells. The fuel cell delivered a P_{\max} value of 150 mW/cm² with an OCV of 1.0 V using BZY as an electrolyte layer between the CF-LBZY cathode and the NCAL anode. On the other hand, the fuel cells produced about 177 mW/cm² with an OCV of 0.96 V using SDC as an electrolyte layer and the CF-LBZY cathode, which is relatively higher than

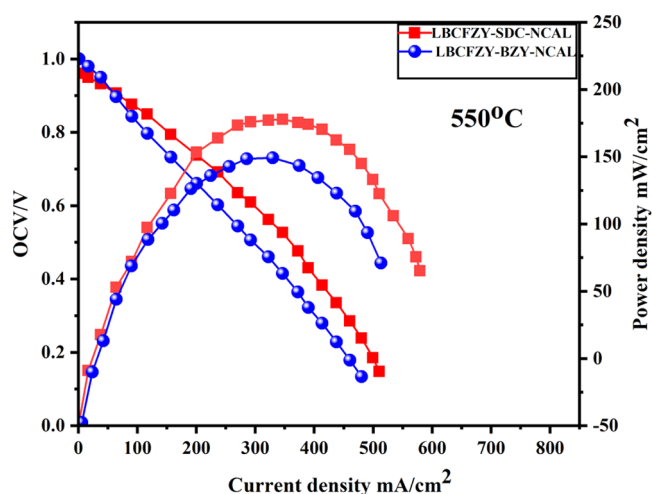


Figure 4. Fuel-cell performance of CF-LBZY/BZY/NCAL and CF-LBZY/SDC/NCAL as an electrode (cathode) at 550 °C.

the conventional fuel cell.³⁶ The abovementioned results suggest that CF-LBZY possesses both the ORR catalytic activity and also confirms triple-charge conduction under low temperature. Furthermore, the use of SDC as an electrolyte and CF-LBZY as a cathode delivered more active sites for the ORR catalytic activity, which aided in enhancing the electrochemical fuel-cell performance. Such findings indicate that CF-LBZY has a good ORR catalytic activity, an essential property for fuel cells' high performance.

3.4. Electrochemical Impedance Spectroscopy. EIS studies of LBZY and CF-LBZY semiconductors were carried out to investigate the electrical process at a different temperature range of 450–550 °C. From the start, at 550 °C, there is a short straight line in the high-frequency range; also, the EIS spectra line of the current material is composed of a half semicircle, as shown in Figure 5a,b. The crossing of the arc at the X-axis in the high-frequency region gives the Ohmic resistance. The equivalent circuit $LR_0 - (R_1QPE_{gb})(R_2QPE_c)$ was implemented where R_0 and R_1 , R_2 denote the Ohmic and polarization resistances, respectively. The Ohmic resistance at high frequency (HF) is usually due to the electrolyte, electrodes, and wires connected,³⁹ and Ohmic resistance primarily contributes to oxygen ions and electrons. The alternative region of EIS spectra at higher resistance and low frequency is denoted as $(R_1 + R_2 = R_p)$, where R_1 is the charge-transfer resistance and R_2 is the mass-transfer resistance of electrodes, at the intermediate frequency arc and the low-frequency arc, respectively.

Furthermore, in the low-frequency region, mostly the electrode processes occurred. Also, as temperature increased from 450 to 550 °C, the spectra arc regularly changed into a continuous line, mostly due to the increase in the mobility of oxygen ions and shorter polarization time of charges causing a reduction of resistance concurrently. As the temperature increased, R_0 decreased from 0.28 to 0.13 Ω/cm^2 , though R_1 reduced from 0.92 to 0.05 Ω/cm^2 due to the thermal activation and migration of ions and electrons at the grain boundary; also resistance R_2 has shown a related behavior that signifies an increase in the electrode reaction activity due to an increase in the temperature (450–550 °C). Such an activity has been attributed to the ORR in the cell or the cathode functionality with CF-LBZY that contained the electrolyte/electrode region.^{13,37} This leads to an increase in the ORR kinetics

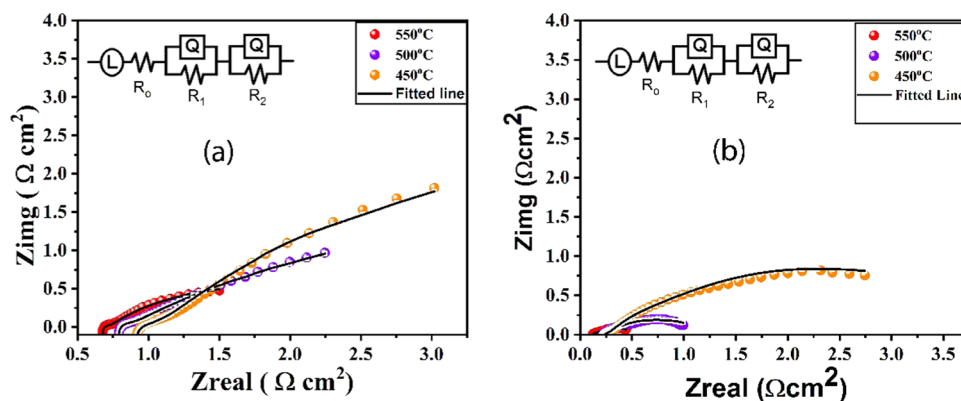


Figure 5. (a) Nyquist plot of Ni-NCAL-LBZY-NCAL-Ni and (b) Nyquist plot for Ni-NCAL-CF-LBZY-NCAL-Ni at 450, 500, and 550 °C.

Table 1. EIS Fitted Data of LBZY and CF-LBZY Obtained Via ZSimpWin Software

composition (°C)	inductance (L)	R_0 (Ω/cm^2)	R_1 (Ω/cm^2)	Q	n	C_1	R_2 (Ω/cm^2)	Q	n	C_2	
LBZY											
550	1.07×10^{-8}	0.68	0.24	0.59	0.20	0.071	0.59	1.27	0.49	0.94	
500	1.144×10^{-7}	0.79	0.35	0.003	0.66	0.00015	1.09	1.23	0.57	1.53	
450	9.15×10^{-8}	0.93	0.55	0.04	1	0.04	1.52	0.28	0.29	0.036	
CF-LBZY											
550	7.99×10^{-8}	0.13	0.05	0.22	0.69	0.036	0.26	1.65	0.58	0.89	
500	2.459×10^{-7}	0.24	0.26	0.48	0.42	0.027	0.49	0.83	0.16	0.0073	
450	1.219×10^{-7}	0.28	0.92	0.00021	1	0.00021	1.5	0.13	0.48	0.022	

activity at the interface of CF-LBZY/NCAL, and is better than that in the undoped LBZY electrolyte layer, as shown in Figure Sa,b. The capacitance has been calculated via the following formula $C_i = \frac{(R_i \times Q_i)^{1/n}}{R_i}$. In addition, the values obtained for LBZY and CF-LBZY from the fitted equivalent circuit $LR_1(QR_2)(QR_3)$ using ZSimpWin software are given in Table 1.

The ionic conductivity of the CF-LBZY material cell can be calculated using the Ohmic resistance value from the I - V curve of electrochemical performance, as reported.^{38–40} The ionic conductivity of the current investigated material is 0.2 S/cm at 550 °C; others covering a temperature range of 450–550 °C are presented in Figure 6. It has also been noticed that by incorporation of Co and Fe, there is an increase in the ionic

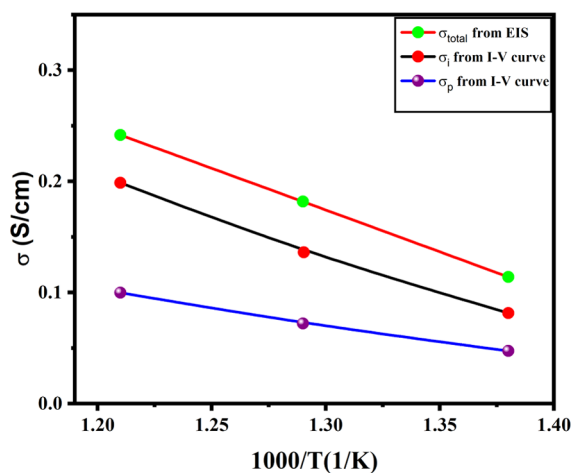


Figure 6. Total and hybrid (i and p) conductivity of cell materials at 450, 500, and 550 °C.

conduction, which might be due to increased oxygen vacancies.^{41–43} The obtained high conductivity is extraordinarily higher than the stated values of oxide-ion conductors, such as SDC \sim 0.05 S/cm, GDC \sim 0.04 S/cm at 700 °C, and YSZ \sim 0.13 S/cm at 1000 °C, and also more significant than the pure proton conductor with BCZY \sim 0.02 S/cm at 700 °C.^{44–48} The conductive properties of the current electrolyte are also temperature-dependent because it has been perceived that the semiconductor electrolyte conductivity increases with temperature, as observed in the semiconductor materials.⁴⁹

CF-LBZY can be a successful candidate the same as BCFZY for proton-conducting fuel cell (PCFC) in many forms, such as high ionic and protonic conductivity and high ORR catalytic activity at low temperature, as confirmed in the literature.⁵⁰ So it is believed that such a high ionic conductivity was the sum of H^+ / O^{2-} conductivities, as reported in the previous report.⁵ Additionally, the thermally activated ions follow the Arrhenius equation in the case ionic flow represented as $\sigma T = A \exp[-E_a/(kT)]$, where σ_i and σ_p are the ionic conduction and protonic conduction, as shown in Figure 6. The ionic conductor, calculated activation energy from the I - V curve, is about 0.68 eV, which is lower than that of other ionic conductors.⁴⁸

As reported previously, BCFZY is a triple conducting material but dominated by proton conduction.^{19,51} The CF-LBZY material developed here showed proton conduction and the highest ionic conduction. From the result, it can be noted that the proton conduction has significantly contributed to the total ionic conduction, which confirms the presence of the triple-charge ($(H^+/O^{2-})/e^-$ or h) conduction, as shown in Figure 6. In addition, the ionic flow is enhanced by suppressing the electronic flow via interfacial conduction at an electrode/electrolyte region that causes to build gradient energy, which separates the ions and electrons to avoid the short-circuiting

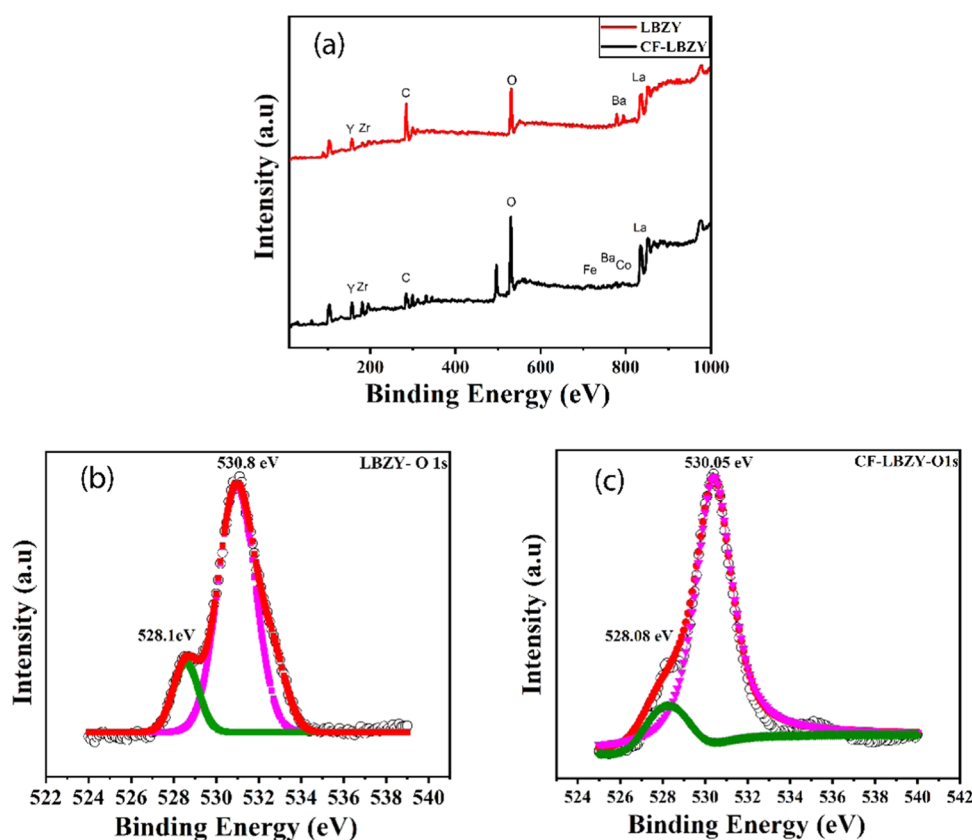


Figure 7. (a) XPS spectra analysis of LBZY and CF-LBZY sample SOFCs. (b, c) Oxygen peaks of LBZY and CF-LBZY elemental analysis, respectively.

problem, leading to the enhancement in the ionic conduction.^{13,37}

3.5. X-ray Photoelectron Spectroscopy. To determine the chemical state with a quantum number, purity, and composition of the single-phase CF-LBZY material, XPS analysis was carried out. The full spectra of XPS of LBZY and CF-LBZY confirm the coexistence of La, Ba, Co, Fe, Zr, Y, and O elements in CF-LBZY, as shown in Figure 7a. In addition, HR (high-resolution) XPS spectra of O 1s are presented in Figure 7b,c, respectively. According to the literature, any material's ionic conduction is closely related to the O 1s BE.^{52–54} Barr and Dong et al. reported that this BE range (528–529.5 eV) was attributed to the most ionic oxides.^{20,33} The peak at 530.5 eV of the undoped LBZY represents the lattice oxygen, while the peak of CF-doped LBZY at 530.8 eV denotes the OH ions, which helps to form O vacancies. The peak at 535 eV was observed, which corresponds to the Na Auger peak that might appear due to the use of Na₂CO₃ during the synthesis process. So, it has been noticed that doping enhances the O vacancies, causing an increase in the ionic conductivity of the material, as shown in Figure 7b,c. These peaks suggest that CF-LBZY has excellent ionic conductivity.

3.6. Electronic Subtraction Via the Metal–Semiconductor (M–S) Junction. The abovementioned results confirm that the CF-LBZY semiconductor perovskite has successfully been applied as an electrolyte with impressive fuel-cell performance and high ionic conductivity for the application of LT-SOFC/CFC. According to the conventional knowledge toward electrochemistry, semiconductor materials possess e-conduction that is not suitable for the electrolyte of the SOFC/CFC device. The e-conduction from an anode to a

semiconductor electrolyte causes profound loss in the form of reduced OCV and fuel-cell performance, leading to short-circuiting.^{36,55} However, interestingly, our results confirm the feasibility of using the CF-LBZY semiconductor as an electrolyte for SOFC/CFC to gain a remarkable performance along with higher OCV > 1 V. These findings suggest that the e-conduction passage from the anode Ni-NCAL to the CF-LBZY semiconductor was congested due some phenomena taking place during the fuel-cell operation.

According to the published literature, the injection of H₂ causes reduction at the anode (NCAL) side of SOFC/CFC.⁵⁶ As a result, it creates Ni/Co metallic alloy at the interface of an electrode (anode), and an electrolyte might cause some interaction among Ni/CF-LBZY. Pondering the semiconducting nature of the CF-LBZY electrolyte, it can be inferred that metal–semiconductor contact is established between Ni/Co–CF-LBZY. Such contact interaction is possibly set up by a Schottky junction, which includes the space–charge region that inhibits the passage of electronic conduction. M–S contacts contain Schottky and Ohmic contacts, which can be recognized using the work function (ϕ) of metals Φ_M and semiconductor Φ_S . The distance between Fermi and vacuum levels is known as the work function either for metal or a semiconductor. In the following case, $\Phi_M > \Phi_S$ semiconductor and metal might establish a contact, leading to leaving the electrons (near to metal) from the semiconductor until establishing a thermal-equilibrium condition again. M–S contacts lead to the depletion of electrons and creation of a space–charge region, which hinder the further transition of electrons across the contact region known as the Schottky junction.⁵⁷ To confirm Schottky junction (Ni/Co electrolyte)

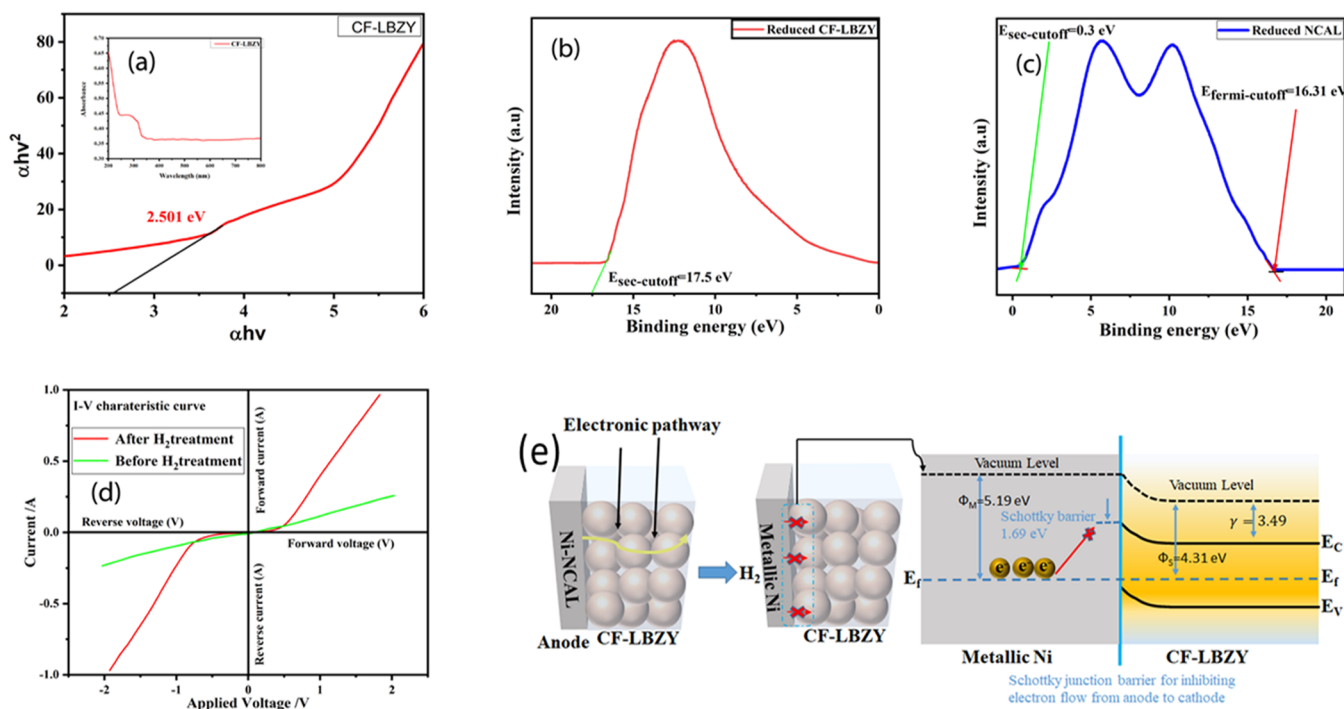


Figure 8. (a–c) UV–visible spectra of CF-LBZY, UPS spectra of CF-LBZY and NCAL pellets treated under H_2 at $550\text{ }^\circ\text{C}$, (d, e) I – V characteristics curve of half-cell NCAL/CF-LBZY tested at $550\text{ }^\circ\text{C}$ prior and after supply of H_2 , and (e) mechanism of suppressing the e-conduction and establishment of the Schottky junction at the anode/electrolyte interface.

formation in our device, UPS spectra (under H_2 treatment at $550\text{ }^\circ\text{C}$ for 4 h) of NCAL and CF-LBZY were obtained and are shown in Figure 8b,c. The calculated work function (based on secondary and Fermi level cutoff) values of reduced NCAL and CF-LBZY are 5.19 and 4.31 eV.

Following the rule mentioned earlier, $\Phi_M > \Phi_S$, the attained work function values confirm the formation of Schottky contact among metal and semiconductor electrolyte layers (Ni/Co–CF-LBZY). The Schottky barrier height was determined by taking the difference of Φ_M and electron affinity γ of the semiconductor electrolyte to show the blocking effect of the Schottky junction at the interface of Ni/Co and CF-LBZY layers.⁵⁷ So, the band gap of CF-LBZY (2.501 eV) under H_2 treatment for 4 h at 550° was elucidated using UV–visible spectroscopy, as shown in Figure 8a. The valence band of the treated CF-LBZY was estimated using the UPS results, leading to the electron-affinity ($\gamma = 3.49\text{ eV}$) value of CF-LBZY. The electron affinity and work function of metal give rise to the barrier height value (1.69 eV) for the metal/CF-LBZY Schottky junction, which leads to creating the potential barrier for inhibiting electronic conduction.

It is important to know that the states (interface states) residing in the M–S contact region might weaken the Schottky contacts and cause it to alternate to the Ohmic contact during the fuel-cell operation. Therefore, to confirm the existence or the establishment of Schottky contact, the I – V characteristics of the half cell (NCAL–Ni/CF-LBZY) were measured at $550\text{ }^\circ\text{C}$. The current response was recorded by applying the bias voltage (-2 to 2 V) to the half cell. At first, the I – V curve characteristics were evaluated without H_2 . Later, H_2 was supplied to the NCAL side to form the metallic Ni/Co and the voltage response was measured by providing the protective gas N_2 , which keeps the cell in a static state during the whole operation. As shown in Figure 8d, before supplying H_2 , there

was no junction effect between the anode and the electrolyte, while as H_2 was supplied to NCAL, the I – V curve showed rectification behavior. Under the reverse bias voltage (-1 to 0 V), the device shows little saturation in the current response, and under a higher bias voltage ($>-1\text{ V}$), the current increased rapidly, which is well suited to the Schottky equation. These results verify the establishment of the Schottky junction between reduced NCAL (metallic phase) and CF-LBZY.

Figure 8e reveals the schematic diagram of the electron inhibiting process in our device and the formation of the Schottky junction at the NCAL/CF-LBZY interface, where the Schottky barrier is considered as the main role player, suppressing the electronic conduction. Figure 8e shows that before the supply of H_2 , a continuous flow of electrons was seen, but as H_2 was supplied, it reduced NCAL to metallic Ni/Co and formed the Schottky junction.^{57,58} Using the attained value of work function, electron-affinity energy-band diagram was constructed between the metal and semiconductor Ni/Co/CF-LBZY, as shown in Figure 8e. The functionality of the barrier height is to suppress the electronic conduction from the anode to the electrolyte, leading to the evasion of fuel-cell short-circuiting issue and guaranteeing the higher OCV and impressive fuel-cell performance.

3.7. Durability Test. To demonstrate the long-term operation of the fuel cell based on CF-LBZY, the durability of the cells was evaluated at $550\text{ }^\circ\text{C}$ under fuel-cell operating conditions shown in Figure 9. The results show 30 h of stable performance with a high and constant current density of 100 mA/cm^2 and an OCV of 0.83 V at $550\text{ }^\circ\text{C}$. From the starting point, the OCV decreased sharply for almost 2 h until it reached a stable point without any degradation. This decrease in voltage at the start of the durability test was because of the stabilization time required for the cell. This fluctuation happened due to the assembly of cell Ni–NCAL–CF-LBZY–

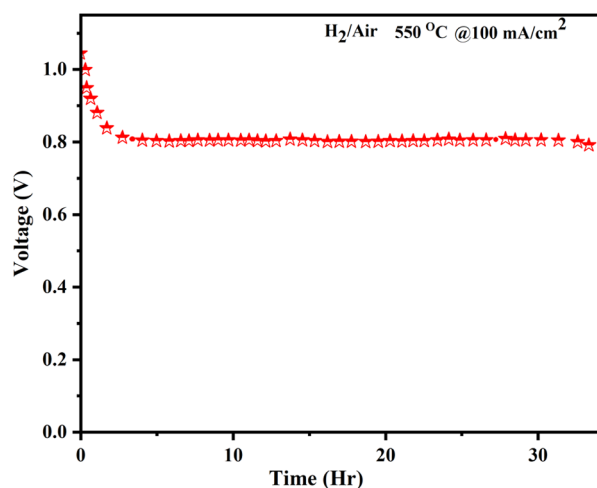


Figure 9. Stability measurement of CF-LBZY CFC at 550 °C for 32 h.

NCAL-Ni materials. Also, the interface gap between an electrode/electrolyte might cause an initial activation process that leads to a small drop in OCV until the gap was spanned with the flow of ions to continue the cell's operation. In addition, there is one main possible reason, which could be the densification of the electrolyte layer. In the beginning, the electrolyte layer is not dense enough and can cause gas leakage, but with time, the voltage gets stable with online densification. A more sophisticated test setup would be required outside the present study's scope for more extended stability tests.

4. CONCLUSIONS

In summary, a single-phase, triple-charge conducting ($O^{2-}/H^+/e^-$) semiconductor oxide for fuel-cell use is presented in this work. A novel perovskite semiconductor $Co_{0.2}/Fe_{0.2}$ -codoped $La_{0.5}Ba_{0.5}Zr_{0.3}Y_{0.3}O_{3-\delta}$ (CF-LBZY) was successfully prepared using the hydrothermal coprecipitation method. The material was used as an electrolyte and an electrode for advanced LT-CFCs. The ionic conductivity and the power density of the fuel cells using this material were high (0.2 S/cm and 656 mW/cm²) at 550 °C but still showed a good performance of 285 mW/cm² at 450 °C. Codoping significantly contributed to the high ionic conduction. From the XPS results, we can conclude that the high concentration of oxygen vacancies in the CF-LBZY samples leads to enhanced visible-light absorption capability. The interpretation of higher OCV and power output in our device have been certified by measuring the work function and electron affinity to explain the electronic suppression based on phenomena of the Schottky junction. The developed CF-LBZY semiconductor materials can be promising alternatives for future LT-CFCs.

AUTHOR INFORMATION

Corresponding Authors

Bin Zhu – Jiangsu Provincial Key Laboratory of Solar Energy Science and Technology/Energy Storage Joint Research Center, School of Energy and Environment, Southeast University, Nanjing 210096, China; orcid.org/0000-0003-1479-0464; Email: binzhu@kth.se

Yuzheng Lu – School of Electronic Engineering, Nanjing Xiaozhuang University, Nanjing 211171, China; Email: mrluyuzheng@163.com

Muhammad Imran Asghar – Hubei Collaborative Innovation Center for Advanced Organic Chemical Materials, Faculty of Physics and Electronic Science, Hubei University, Wuhan, Hubei 430062, China; New Energy Technologies Group, Department of Applied Physics, Aalto University School of Science, FI-00076 Espoo, Finland; orcid.org/0000-0003-3559-0955; Email: imran.asghar@aalto.fi

Authors

M. A. K. Yousaf Shah – Engineering Research Center of Nano-Geo Materials of Ministry of Education, Department of Materials Science and Chemistry, China University of Geosciences, Wuhan 430074, China; orcid.org/0000-0002-1081-9090

Sajid Rauf – Hubei Collaborative Innovation Center for Advanced Organic Chemical Materials, Faculty of Physics and Electronic Science, Hubei University, Wuhan, Hubei 430062, China

Naveed Mushtaq – Hubei Collaborative Innovation Center for Advanced Organic Chemical Materials, Faculty of Physics and Electronic Science, Hubei University, Wuhan, Hubei 430062, China; Jiangsu Provincial Key Laboratory of Solar Energy Science and Technology/Energy Storage Joint Research Center, School of Energy and Environment, Southeast University, Nanjing 210096, China

Zuhra Tayyab – Hubei Collaborative Innovation Center for Advanced Organic Chemical Materials, Faculty of Physics and Electronic Science, Hubei University, Wuhan, Hubei 430062, China

Muhammad Yousaf – Hubei Collaborative Innovation Center for Advanced Organic Chemical Materials, Faculty of Physics and Electronic Science, Hubei University, Wuhan, Hubei 430062, China; Jiangsu Provincial Key Laboratory of Solar Energy Science and Technology/Energy Storage Joint Research Center, School of Energy and Environment, Southeast University, Nanjing 210096, China

Muhammad Bilal Hanif – State Key Laboratory for Mechanical Behavior of Materials, School of Materials Science and Engineering, Xi'an Jiaotong University, Xi'an 710061, Shaanxi, China

Peter D. Lund – Jiangsu Provincial Key Laboratory of Solar Energy Science and Technology/Energy Storage Joint Research Center, School of Energy and Environment, Southeast University, Nanjing 210096, China; New Energy Technologies Group, Department of Applied Physics, Aalto University School of Science, FI-00076 Espoo, Finland; orcid.org/0000-0002-4819-3847

Complete contact information is available at: <https://pubs.acs.org/10.1021/acsaem.1c00599>

Author Contributions

^VM.A.K.Y.S., S.R., and N.M. contributed equally to this work.

Notes

The authors declare no competing financial interest.

ACKNOWLEDGMENTS

This work was supported by the National Natural Science Foundation of China (NSFC, Grant Nos. 51774259, 51772080, and 51675496) and the Engineering Research Center of Nano-Geo Materials of Ministry of Education (NGM2017KF004, NGM2017KF012, and NGM2018KF016). Dr. Asghar acknowledges the support from the Hubei overseas

Talent 100 program (as a distinguished professor at Hubei University) and the Academy of Finland (Grant No. 13329016, 13322738) for their support.

REFERENCES

- (1) Wachsmann, E. D.; Lee, K. T. Lowering the temperature of solid oxide fuel cells. *Science* **2011**, *334*, 935–939.
- (2) Ding, C.; Hashida, T. High performance anode-supported solid oxide fuel cell based on thin-film electrolyte and nanostructured cathode. *Energy Environ. Sci.* **2010**, *3*, 1729–1731.
- (3) Nomura, H.; Parekh, S.; Selman, J. R.; Al-Hallaj, S. Fabrication of YSZ electrolyte for intermediate temperature solid oxide fuel cell using electrostatic spray deposition: II—Cell performance. *J. Appl. Electrochem.* **2005**, *35*, 1121–6.
- (4) Will, J.; Mitterdorfer, A.; Kleinlogel, C.; Perednis, D.; Gauckler, L. J. Fabrication of thin electrolytes for second-generation solid oxide fuel cells. *Solid State Ionics* **2000**, *131*, 79–96.
- (5) Zhang, C.; Zhao, H. Structural characteristics, sinterability and electrical conductivity of Ba-site non-stoichiometric $Ba_xCe_{1-x}O_{3-\delta}$. *Mater. Res. Bull.* **2010**, *45*, 1659–1663.
- (6) Asghar, M. I.; Heikkilä, M.; Lund, P. D. Advanced low-temperature ceramic nanocomposite fuel cells using ultra high ionic conductivity electrolytes synthesized through freeze-dried method and solid-route. *Mater. Today Energy* **2017**, *5*, 338–346.
- (7) Khan, I.; Asghar, M. I.; Lund, P. D.; Basu, S. High conductive (LiNaK) $2CO_3Ce_{0.85}Sm_{0.15}O_2$ electrolyte compositions for IT-SOFC applications. *Int. J. Hydrogen Energy* **2017**, *42*, 20904–20909.
- (8) Asghar, M. I.; Jouttijärvi, S.; Jokiranta, R.; Valtavirta, A. M.; Lund, P. D. Wide bandgap oxides for low-temperature single-layered nanocomposite fuel cell. *Nano Energy* **2018**, *53*, 391–397.
- (9) Zhou, W.; Shao, Z. Fuel cells: hydrogen induced insulation. *Nat. Energy* **2016**, *1*, No. 16078.
- (10) Fabbri, E.; Bi, L.; Pergolesi, D.; Traversa, E. Towards the next generation of solid oxide fuel cells operating below 600 °C with chemically stable proton-conducting electrolytes. *Adv. Mater.* **2012**, *24*, 195–208.
- (11) Mather, G. C.; Fisher, C. A.; Islam, M. S. Defects, dopants, and protons in $LaNbO_4$. *Chem. Mater.* **2010**, *22*, 5912–5917.
- (12) Zhao, J.; Xu, X.; Zhou, W.; Blakey, I.; Liu, S.; Zhu, Z. Proton-conducting La-doped ceria-based internal reforming layer for direct methane solid oxide fuel cells. *ACS Appl. Mater. Interfaces* **2017**, *9*, 33758–33765.
- (13) Duan, C.; Tong, J.; Shang, M.; Nikodemski, S.; Sanders, M.; Ricote, S.; Almansoori, A.; O’Hayre, R. Readily processed protonic ceramic fuel cells with high performance at low temperatures. *Science* **2015**, *349*, 1321–1326.
- (14) Ganesh, K. S.; Wang, B.; Kim, J. S.; Zhu, B. Ionic conducting properties and fuel cell performance developed by band structures. *J. Phys. Chem. C* **2019**, *123*, 8569–8577.
- (15) Bae, K.; Jang, D. Y.; Choi, H. J.; Kim, D.; Hong, J.; Kim, B. K.; Lee, J. H.; Son, J. W.; Shim, J. H. Demonstrating the potential of yttrium-doped barium zirconate electrolyte for high-performance fuel cells. *Nat. Commun.* **2017**, *8*, No. 14553.
- (16) Zhou, Y.; Guan, X.; Zhou, H.; Ramadoss, K.; Adam, S.; Liu, H.; Lee, S.; Shi, J.; Tsuchiya, M.; Fong, D. D.; Ramanathan, S. Strongly correlated perovskite fuel cells. *Nature* **2016**, *534*, 231–234.
- (17) Chen, G.; Liu, H.; He, Y.; Zhang, L.; Asghar, M. I.; Geng, S.; Lund, P. D. Electrochemical mechanisms of an advanced low-temperature fuel cell with a $SrTiO_3$ electrolyte. *J. Mater. Chem. A* **2019**, *7*, 9638–9645.
- (18) Chen, G.; Zhu, B.; Deng, H.; Luo, Y.; Sun, W.; Liu, H.; Zhang, W.; Wang, X.; Qian, Y.; Hu, X.; Geng, S.; et al. Advanced fuel cell based on perovskite $La-SrTiO_3$ Semiconductor as the electrolyte with superoxide-ion conduction. *ACS Appl. Mater. Interfaces* **2018**, *10*, 33179–33186.
- (19) Xia, C.; Mi, Y.; Wang, B.; Lin, B.; Chen, G.; Zhu, B. Shaping triple-conducting semiconductor $BaCo_{0.4}Fe_{0.4}Zr_{0.1}Y_{0.1}O_{3-\delta}$ into an electrolyte for low-temperature solid oxide fuel cells. *Nat. Commun.* **2019**, *10*, No. 1707.
- (20) Dong, W.; Tong, Y.; Zhu, B.; Xiao, H.; Wei, L.; Huang, C.; Wang, B.; Wang, X.; Kim, J. S.; Wang, H. Semiconductor TiO_2 thin film as an electrolyte for fuel cells. *J. Mater. Chem. A* **2019**, *7*, 16728–16734.
- (21) Shah, M. A. K. Y.; Mushtaq, N.; Rauf, S.; Xia, C.; Zhu, B. The semiconductor $SrFeO_{2-x}TiO_{3-\delta}$ heterostructure electrolyte fuel cells. *Int. J. Hydrogen Energy* **2019**, *44*, 30319–30327.
- (22) Yamazaki, Y.; Hernandez-Sanchez, R.; Haile, S. M. High total proton conductivity in large-grained yttrium-doped barium zirconate. *Chem. Mater.* **2009**, *21*, 2755–2762.
- (23) Shah, M. A. K. Y.; Zhu, B.; Rauf, S.; Mushtaq, N.; Yousaf, M.; Ali, N.; Tayyab, Z.; Akbar, N.; Yang, C. P.; Wang, B. Electrochemical Properties of a Co-Doped $SrSnO_3-\delta$ -Based Semiconductor as an Electrolyte for Solid Oxide Fuel Cells. *ACS Applied Energy. Materials* **2020**, *3*, 6323–6333.
- (24) Rauf, S.; Zhu, B.; Yousaf Shah, M. A.; Tayyab, Z.; Attique, S.; Ali, N.; Mushtaq, N.; Wang, B.; Yang, C.; Asghar, M. I.; Lund, P. D. Application of a Triple-Conducting Heterostructure Electrolyte of $Ba_{0.5}Sr_{0.5}Co_{0.1}Fe_{0.7}Zr_{0.1}Y_{0.1}O_{3-\delta}$ and $Ca_{0.04}Ce_{0.8}Sm_{0.16}O_{2-\delta}$ in a High-Performance Low-Temperature Solid Oxide Fuel Cell. *ACS Appl. Mater. Interfaces* **2020**, *12*, 35071–35080.
- (25) Rauf, S.; Shah, M. Y.; Ali, N.; Mushtaq, N.; Tayyab, Z.; Yousaf, M.; Yang, C. P.; Wang, B. Tuning semiconductor $LaFeO_{3-\delta}$ to fast ionic transport for advanced ceramics fuel cells. *Int. J. Hydrogen Energy* **2020**, *46*, 9861–9873.
- (26) Shah, M. A. K. Y.; Mushtaq, N.; Rauf, S.; Akbar, N.; Xing, Y.; Wu, Y.; Wang, B.; Zhu, B. Advanced fuel cell based on semiconductor perovskite $La-BaZrY_3O_{7-\delta}$ as an electrolyte material operating at low temperature 550 °C. *Int. J. Hydrogen Energy* **2020**, *45*, 27501–27509.
- (27) Shah, M. A. K. Y.; Rauf, S.; Mushtaq, N.; Tayyab, Z.; Ali, N.; Yousaf, M.; Xing, Y.; Akbar, M.; Lund, P. D.; Yang, C. P.; Zhu, B.; et al. Semiconductor Fe-doped $SrTiO_3-\delta$ perovskite electrolyte for low-temperature solid oxide fuel cell (LT-SOFC) operating below 520 °C. *Int. J. Hydrogen Energy* **2020**, *45*, 14470–14479.
- (28) Shao, K.; Li, F.; Zhang, G.; Zhang, Q.; Maliutina, K.; Fan, L. Approaching durable single-layer fuel cells: promotion of electroactivity and charge separation via nanoalloy redox exsolution. *ACS Appl. Mater. Interfaces* **2019**, *11*, 27924–27933.
- (29) Fan, L.; Zhu, B.; Su, P. C.; He, C. Nanomaterials and technologies for low temperature solid oxide fuel cells: recent advances, challenges and opportunities. *Nano Energy* **2018**, *45*, 148–176.
- (30) Shah, M. A. K. Y.; Rauf, S.; Zhu, B.; Mushtaq, N.; Yousaf, M.; Lund, P. D.; Xia, C.; Asghar, M. I. Semiconductor Nb-Doped $SrTiO_3-\delta$ Perovskite Electrolyte for a Ceramic Fuel Cell. *ACS Appl. Energy Mater.* **2021**, *4*, 365–375.
- (31) Xing, Y.; Wu, Y.; Li, L.; Shi, Q.; Shi, J.; Yun, S.; Akbar, M.; Wang, B.; Kim, J. S.; Zhu, B. Proton shuttles in $CeO_2/CeO_{2-\delta}$ core-shell structure. *ACS Energy Lett.* **2019**, *4*, 2601–2607.
- (32) Meng, Y.; Wang, X.; Zhang, W.; Xia, C.; Liu, Y. N.; Yuan, M.; Zhu, B.; Ji, Y. Novel high ionic conductivity electrolyte membrane based on semiconductor $La_{0.65}Sr_{0.3}Ce_{0.05}Cr_{0.05}Fe_{0.05}O_{3-\delta}$ for low-temperature solid oxide fuel cells. *J. Power Sources* **2019**, *421*, 33–40.
- (33) Xie, K.; Yan, R.; Chen, X.; Dong, D.; Wang, S.; Liu, X.; Meng, G. A new stable $BaCeO_3$ -based proton conductor for intermediate-temperature solid oxide fuel cells. *J. Alloys Compd.* **2009**, *472*, 551–555.
- (34) Fabbri, E.; Bi, L.; Tanaka, H.; Pergolesi, D.; Traversa, E. Chemically stable Pr and Y co-doped barium zirconate electrolytes with high proton conductivity for intermediate-temperature solid oxide fuel cells. *Adv. Funct. Mater.* **2011**, *21*, 158–166.
- (35) D’Epifanio, A.; Fabbri, E.; Di Bartolomeo, E.; Licocchia, S.; Traversa, E. Design of $BaZr_{0.8}Y_{0.2}O_{3-\delta}$ Protonic Conductor to Improve the Electrochemical Performance in Intermediate Temperature Solid Oxide Fuel Cells (IT-SOFCs). *Fuel Cells* **2008**, *8*, 69–76.

- (36) Shen, S.; Yang, Y.; Guo, L.; Liu, H. A polarization model for a solid oxide fuel cell with a mixed ionic and electronic conductor as electrolyte. *J. Power Sources* **2014**, *256*, 43–51.
- (37) He, W.; Wu, X.; Yang, G.; Shi, H.; Dong, F.; Ni, M. BaCo_{0.7}Fe_{0.22}Y_{0.08}O_{3-δ} as an active oxygen reduction electrocatalyst for low-temperature solid oxide fuel cells below 600 °C. *ACS Energy Lett.* **2017**, *2*, 301–305.
- (38) Xia, C.; Qiao, Z.; Shen, L.; Liu, X.; Cai, Y.; Xu, Y.; Qiao, J.; Wang, H. Semiconductor electrolyte for low-operating-temperature solid oxide fuel cell: Li-doped ZnO. *Int. J. Hydrogen Energy* **2018**, *43*, 12825–12834.
- (39) Zhu, B. Using a fuel cell to study fluoride-based electrolytes. *Electrochem. Commun.* **1999**, *1*, 242–246.
- (40) Fan, L.; Wang, C.; Chen, M.; Di, J.; Zheng, J.; Zhu, B. Potential low-temperature application and hybrid-ionic conducting property of ceria-carbonate composite electrolytes for solid oxide fuel cells. *Int. J. Hydrogen Energy* **2011**, *36*, 9987–9993.
- (41) Ishihara, T.; Akbay, T.; Furutani, H.; Takita, Y. Improved oxide ion conductivity of Co doped La_{0.8}Sr_{0.2}Ga_{0.8}Mg_{0.2}O₃ perovskite type oxide. *Solid State Ionics* **1998**, *113–115*, 585–591.
- (42) Li, M.; Wu, R.; Zhu, L.; Cheng, J.; Hong, T.; Xu, C. Enhanced sinterability and conductivity of cobalt doped lanthanum niobate as electrolyte for proton-conducting solid oxide fuel cell. *Ceram. Int.* **2019**, *45*, 573–578.
- (43) Lai, H. Y.; Chan, Y. H.; et al. Enhancement of ion conductivity for doped electrolytes in SOFC by MD modeling. *Comput. Mater. Sci.* **2018**, *144*, 265–272.
- (44) Garbayo, I.; Baiutti, F.; Morata, A.; Tarancon, A. Engineering mass transport properties in oxide ionic and mixed ionic-electronic thin film ceramic conductors for energy applications. *J. Eur. Ceram. Soc.* **2019**, *39*, 101–114.
- (45) Prabhakaran, K.; Beigh, M. O.; Lakra, J.; Gokhale, N. M.; Sharma, S. C. Characteristics of 8 mol% yttria stabilized zirconia powder prepared by spray drying process. *J. Mater. Process. Technol.* **2007**, *189*, 178–181.
- (46) Fu, Y. P.; Wen, S. B.; Lu, C. H. Preparation and characterization of samaria-doped ceria electrolyte materials for solid oxide fuel cells. *J. Am. Ceram. Soc.* **2008**, *91*, 127–131.
- (47) Fabbri, E.; D'Epifanio, A.; Di Bartolomeo, E.; Licoccia, S.; Traversa, E. Tailoring the chemical stability of Ba (Ce_{0.8-x}Zr_x)Y_{0.2}O_{3-δ} protonic conductors for intermediate temperature solid oxide fuel cells (IT-SOFCs). *Solid State Ionics* **2008**, *179*, 558–564.
- (48) Wei, T.; Singh, P.; Gong, Y.; Goodenough, J. B.; Huang, Y.; Huang, K. Sr_{3-3x}Na_{3x}Si₃O_{9-1.5x} (x = 0.45) as a superior solid oxide-ion electrolyte for intermediate temperature-solid oxide fuel cells. *Energy Environ. Sci.* **2014**, *7*, 1680–1684.
- (49) Yoon, H. S.; Choi, S. W.; Lee, D.; Kim, B. H. Synthesis and characterization of Gd_{1-x}Sr_xMnO₃ cathode for solid oxide fuel cells. *J. Power Sources* **2001**, *93*, 1–7.
- (50) An, H.; Lee, H.-W.; Kim, B.-K.; Son, J.-W.; Yoon, K. J.; Kim, H.; Shin, D.; Ji, H.-I.; Lee, J.-H. A 5 × 5 cm² protonic ceramic fuel cell with a power density of 1.3 W cm⁻² at 600 °C. *Nat. Energy* **2018**, *3*, 870.
- (51) Ren, R.; Wang, Z.; Xu, C.; Sun, W.; Qiao, J.; Rooney, D. W.; Sun, K. Tuning the defects of the triple conducting oxide BaCo_{0.4}Fe_{0.4}Zr_{0.1}Y_{0.1}O_{3-δ} perovskite toward enhanced cathode activity of protonic ceramic fuel cells. *J. Mater. Chem. A* **2019**, *7*, 18365–18372.
- (52) Dimitrov, V.; Komatsu, T. Classification of simple oxides: a polarizability approach. *J. Solid State Chem.* **2002**, *163*, 100–112.
- (53) Barr, T. L. Modern ESCA. In *Photoelectron Spectroscopy*; CRC Press, 1994.
- (54) Pawlak, D. A.; Ito, M.; Oku, M.; Shimamura, K.; Fukuda, T. Interpretation of XPS O (1s) in mixed oxides proved on mixed perovskite crystals. *J. Phys. Chem. B* **2002**, *106*, 504–507.
- (55) Shen, S.; Ni, M. 2D segment model for a solid oxide fuel cell with a mixed ionic and electronic conductor as electrolyte. *Int. J. Hydrogen Energy* **2015**, *40*, 5160–5168.
- (56) Zhu, B.; Lund, P. D.; Raza, R.; Ma, Y.; Fan, L.; Afzal, M.; Patakangas, J.; He, Y.; Zhao, Y.; Tan, W.; Huang, Q. A.; et al. Schottky junction effect on high performance fuel cells based on nanocomposite materials. *Adv. Energy Mater.* **2015**, *5*, No. 1401895.
- (57) Lutz, J.; Schlagenotto, H.; Scheuermann, U.; Doncker, R. Semiconductor Power Devices. In *Physics, Characteristics, Reliability*, 2011; p 2.
- (58) Wang, B.; Cai, Y.; Xia, C.; Kim, J. S.; Liu, Y.; Dong, W.; Wang, H.; Afzal, M.; Li, J.; Raza, R.; Zhu, B. Semiconductor-ionic membrane of LaSrCoFe-oxide-doped ceria solid oxide fuel cells. *Electrochim. Acta* **2017**, *248*, 496–504.